Hindawi
Journal of Nanomaterials
Volume 2019, Article ID 3698326, 8 pages
https://doi.org/10.1155/2019/3698326

Research Article

Catalytic Properties of Phosphate-Coated $CuFe_2O_4$ Nanoparticles for Phenol Degradation

Israa Othman,[1] Mohammad Abu Haija ,[1] and Fawzi Banat[2]

[1]*Department of Chemistry, Khalifa University of Science and Technology, SAN Campus, PO Box 2533, Abu Dhabi, UAE*
[2]*Department of Chemical Engineering, Khalifa University of Science and Technology, SAN Campus, PO Box 2533, Abu Dhabi, UAE*

Correspondence should be addressed to Mohammad Abu Haija; mohammad.abuhaija@ku.ac.ae

Received 12 August 2018; Revised 10 November 2018; Accepted 28 November 2018; Published 3 March 2019

Academic Editor: Jianbo Yin

Copper ferrite ($CuFe_2O_4$) nanoparticles were prepared using the sol-gel autocombustion method and then coated with phosphate using different treatments with H_3PO_4. The structural and chemical properties of the phosphate-coated $CuFe_2O_4$ nanoparticles were controlled by changing the concentration of H_3PO_4 during the coating process. The prepared nanoparticles were characterized using XRD, FTIR, SEM, and EDS which provided information about the catalysts' structure, chemical composition, purity, and morphology. The catalytic and photocatalytic activities of the phosphate-coated $CuFe_2O_4$ samples were tested and evaluated for the degradation of phenol using HPLC. The prepared nanoparticles successfully emerged as excellent heterogeneous Fenton-type catalysts for phenol degradation. The phosphate-coated $CuFe_2O_4$ catalysts exhibited a higher catalytic activity compared with the uncoated $CuFe_2O_4$ ones. Such a higher catalytic performance can be attributed to enhanced morphological, electronic, and chemical properties of the phosphate-coated $CuFe_2O_4$ nanoparticles. Additionally, the phosphate-coated $CuFe_2O_4$ nanoparticles also revealed a higher catalytic activity compared with TiO_2 nanoparticles. Different experimental conditions were investigated, and complete removal of phenol was achieved under specific conditions.

1. Introduction

The rapid development in industries increased the amount of wastewater discharged into water bodies. The discharged wastewater contains different organic and inorganic pollutants which are highly toxic and harmful to the environment. These pollutants resist degradation and are environmentally persistent which required developing new approaches to tackle this problem [1, 2]. The discharged industrial waste contains chemicals like cyanides, mono- or polycyclic aromatics, mercaptans, phenols, ammonia, and sulfides, which are affecting the aquatic habitat via halting algae growth, oxygen depletion, and altering the properties of water [3]. Phenol is one of the abundant hazardous pollutants in wastewater. Phenol was found to be teratogenic, toxic, highly persistent in the environment, and nonbiodegradable [4–6]. Once it is discharged into water bodies, it presents a threat to aquatic systems and its inhabitants as well as humans' health [7]. Phenol in wastewater can be treated by various physical and chemical techniques, such as microwave [8, 9], membrane technology [10], electrochemical [11, 12], thermal [13], and physiochemical processes [14, 15]. One of the most adopted techniques in wastewater treatment is the chemical oxidation including the advanced oxidation processes [3, 16].

Advanced oxidation processes (AOP) include different systems like Fenton, photocatalysis, and UV/H_2O processes, which mostly proceed via active nonselective radicals such as hydroxyl radicals (HO·). The radicals are produced through the decomposition of strong oxidants like hydrogen peroxide. In most of these processes, $HO^{\bullet}$ oxidizes phenol and its derivatives to cyclic intermediates that are converted to organic acids which are then mineralized to CO_2 and H_2O [17]. Recent studies showed that heterogeneous catalysts combined with the advanced oxidation process (AOP) can be used for the degradation of aromatic organic compounds in wastewater [18, 19]. While zeolites, clays, and oxide materials were found to be some of the efficient systems

for the AOP, the most used ones were mixed iron oxide nanoparticles [20–23].

Ferrites are iron oxides with the general formula MFe_2O_4 (M = Ni, Mn, Co, and so on). Spinel ferrites exhibit cubic close packing of oxide ions that form tetrahedral and octahedral coordination, where the divalent metal ions are incorporated. Ferrites have a large number of applications due to their being moderately cheap, highly efficient, recyclable, magnetic, and catalytic properties. They are often used in gas sensors, energy storage, semiconductors, magnetic-based separation, catalysis, and refractory materials. Reactions like decomposition of cyclic organic peroxides, oxidation of propane, oxidation of phenol, and decomposition of hydrogen peroxide are catalyzed by ferrites [13, 24]. Copper ferrites are thermally stable magnetic particles which are frequently employed in various environmental applications. $CuFe_2O_4$ nanoparticles are used as catalysts and gas sensors [19, 25, 26]. Ferrites tend to agglomerate due to van der Waals forces, high surface energy, and magnetic dipolar interaction. One of the solutions employed to overcome this problem is coating [27]. The organic coating includes polyamides, polyvinyl alcohol, epoxy, and silicone resins, while the inorganic coating includes oxides and phosphates. Among these coatings, phosphate stands out for its high electrical resistivity, the simplicity of preparation, and high adhesion to the substance surface [28]. The phosphate coating is often done through a phosphate bath or immersing the material in phosphoric acid to form phosphate layer on its surface.

Phosphate doping has improved the catalytic activities of oxide catalysts such as TiO_2 [29–31] and $BiVO_4$ [32], and, consequently, it is expected to improve the catalytic properties of ferrites. In our previous work [19], $CuFe_2O_4$ nanoparticles were utilized as efficient Fenton-like catalysts for phenol degradation. The main goal of the present work is to investigate the effect of phosphate coating on the structural, chemical, and catalytic properties of the $CuFe_2O_4$ nanoparticles. To our knowledge, there are no reports discussing the catalytic properties of phosphate-coated $CuFe_2O_4$ nanoparticles. The obtained results for the degradation of phenol demonstrated that the prepared nanoparticles exhibited a high Fenton catalytic performance with an almost complete degradation of phenol. The results also revealed that phosphate-coated $CuFe_2O_4$ nanoparticles exhibited higher catalytic activities than pure uncoated $CuFe_2O_4$ ones. The influences of different coating treatments, solution pH, and reaction temperature on the degradation of phenol were investigated. The photocatalytic activity of the phosphate-coated $CuFe_2O_4$ nanoparticles was also examined.

2. Materials and Methods

2.1. Catalyst Preparation. Firstly, pure uncoated $CuFe_2O_4$ nanoparticles were prepared using the sol-gel autocombustion method as described previously [19]. In brief, predetermined amounts of ferric nitrate and the copper (II) nitrate were dissolved in distilled water. Citric acid was then added to the solution and stirred till the acid completely dissolved. The molar ratio of the ferric nitrate, copper (II) nitrate and citric acid was 2 : 1 : 3. After that, the solution was heated to 80°C, and then, ammonia was added until the pH of the solution was around 8. The solution was left to boil until a thick gel was formed, which was kept overnight at room temperature. The gel was then burned and an ash-like product was obtained. The catalyst was crushed and kept for the phosphate-coating step in which the obtained $CuFe_2O_4$ powder was treated with acetone for 15 minutes. After that, the powder was filtered and dried in the oven at 70°C. Then, 0.5 g of the dried $CuFe_2O_4$ powder was treated with 25 mL of 0.35 M, 0.60 M, 0.80 M, 1.20 M, or 1.50 M of H_3PO_4 for 30 minutes at room temperature. The separated powder was dried overnight in an oven at 100°C. Finally, the dried catalyst, phosphate-coated $CuFe_2O_4$, was gently grinded and stored for the study.

Additional comparative studies were carried out using TiO_2 nanoparticles (>99%) purchased from Sigma-Aldrich and used as received.

2.2. Catalyst Characterization. The crystal structures of the uncoated and coated catalysts were determined using X-ray diffraction PANalytical powder diffractometer (X'Pert PRO) which uses Cu-Kα radiation operating at 40 kV and 40 mA at 1.5406 Å, over the 2θ range of 10°-80° and a step size equal to 0.02°. The crystallite sizes were calculated by the Debye-Scherrer formula:

$$L = \frac{K\lambda}{B\cos\theta}, \quad (1)$$

where K is the Scherrer constant (0.89), λ is the wavelength of the XRD instrument, θ is the diffraction angle, B is the peak full width at half maximum of the intensity plotted against the 2θ profile, and L is the crystallite size in nm [33].

The morphologies of the ferrites were analyzed through scanning electron microscopy FEG Quanta 250 provided with energy-dispersive spectrometer (EDS). The FTIR spectra were recorded using a Bruker ALPHA-Platinum ATR FTIR in the range of 400-4000 cm^{-1}.

2.3. Phenol Degradation Reaction. Degradation reactions were carried out in a 150 mL glass beaker containing 95.00 mL of 200 ppm phenol and 5 mL of 30% H_2O_2. The reaction started after adding 60 mg of catalyst to the solution with continuous stirring. At specific time intervals, samples were withdrawn and filtered using 0.2 μm nylon membrane filters. HPLC was used to analyze the samples in order to determine the remaining concentration of phenol. HPLC measurements were conducted using a Shimadzu machine equipped with a UV detector that was set at 280 nm. The HPLC method was previously developed to follow the phenol degradation process [19].

The following formula was used to calculate the degradation efficiency of phenol:

$$\text{Degradation\%} = \frac{(C_o - C_t)}{C_o} \times 100, \quad (2)$$

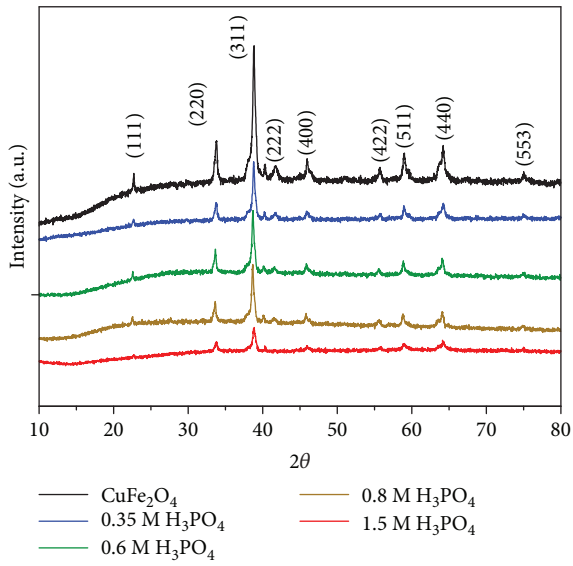

Figure 1: XRD patterns of pure $CuFe_2O_4$ (top) and different phosphate-coated $CuFe_2O_4$ by treatment with 0.35, 0.6, 0.8, and 1.5 M of H_3PO_4.

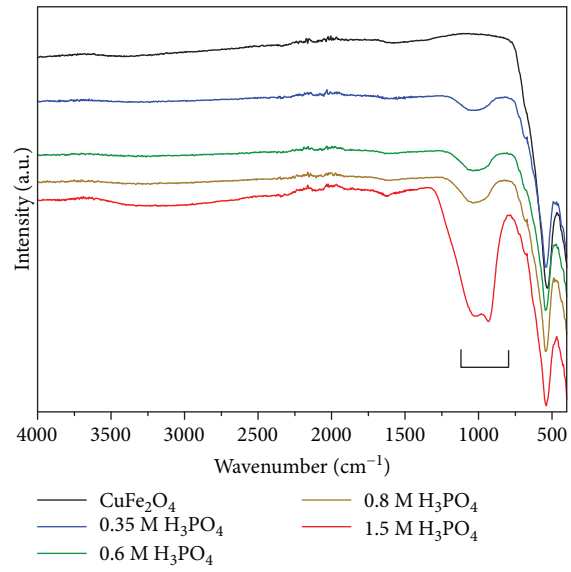

Figure 2: FTIR spectra of pure $CuFe_2O_4$ (top) and different phosphate-coated $CuFe_2O_4$ by treatment with 0.35, 0.6, 0.8, and 1.5 M of H_3PO_4.

where C_o is the initial concentration of phenol and C_t is the remaining concentration of phenol after a specific time of the reaction.

The degradation reactions were modeled using the following first-order expression:

$$\ln \frac{C_t}{C_o} = -kt, \quad (3)$$

where C_o is the initial concentration of phenol, C_t is the residual concentration of phenol after a specific time of the reaction, and k is the rate contact which can be calculated from the slope of $\ln (C_t/C_o)$ versus time.

In order to investigate the photocatalytic activities of the prepared catalysts, similar reactions were carried out using a photocatalytic reactor equipped with a metal halide lamp (OSRAM 400 W, 350-750 nm).

3. Results and Discussion

3.1. Structural Analysis

3.1.1. XRD. XRD patterns of the sol-gel, as-prepared $CuFe_2O_4$ sample, and the phosphate-coated $CuFe_2O_4$ samples are presented in Figure 1. The observed XRD patterns are in agreement with the standard CuFe2O4 data (JCPDS card 77–0010) and with literature reports [19, 34]. The reflection planes (111), (220), (311), (222), (400), (422), (511), (440), and (533) confirm that the $CuFe_2O_4$ samples were crystallites of spinel ferrite with a cubic phase [19]. The $CuFe_2O_4$ nanoparticles maintained their cubic structure even after treatment with phosphoric acid. However, the diffraction peaks are less intense and broader for the sample treated with 1.5 M of phosphoric acid, which may have affected the $CuFe_2O_4$ structure and reduced its crystallinity. Using Scherrer's equation, the crystallite sizes of the samples were in the range of 24-31 nm.

3.1.2. FTIR. IR measurements are commonly conducted for ferrites in order to verify the presence of the spinel phase of the prepared samples. Ferrites exhibit two IR modes in the range of 400-600 cm^{-1} which are attributed to the vibrations of the cations with oxygen ions in the octahedral and tetrahedral sites in the unit cell. The FTIR spectra of the $CuFe_2O_4$ samples are depicted in Figure 2 which clearly shows the typical frequency mode of ferrites at ~600 cm^{-1} due to the stretching vibration of iron-oxygen ions in tetrahedral sites [19, 35]. Moreover, additional absorption peaks are observed in the region of 970–1120 cm^{-1} for the phosphate-coated $CuFe_2O_4$ samples, which are attributed to phosphorus-oxygen stretching vibration [36]. The intensity of these peaks increased with the increase of phosphoric acid concentration from 0.35 to 1.5 M.

3.1.3. SEM. The SEM images of the phosphate-coated $CuFe_2O_4$ samples are depicted in Figure 3. The images of the phosphate-coated $CuFe_2O_4$ samples show sheet-like structures while those of the uncoated $CuFe_2O_4$ samples exhibit a sponge-like structure. The size of these sheets increased with the increase of the concentration of phosphoric acid used for coating. It is also obvious that coating the $CuFe_2O_4$ particles with phosphate increased the surface roughness. The EDS analysis confirmed the presence of phosphorus for each phosphate-coated $CuFe_2O_4$ sample.

3.2. Phenol Degradation Reactions. Initially, the nonphotocatalytic performance of the prepared catalysts was investigated at room temperature. The obtained results, displayed in Figure 4, clearly show that phosphate-coated $CuFe_2O_4$

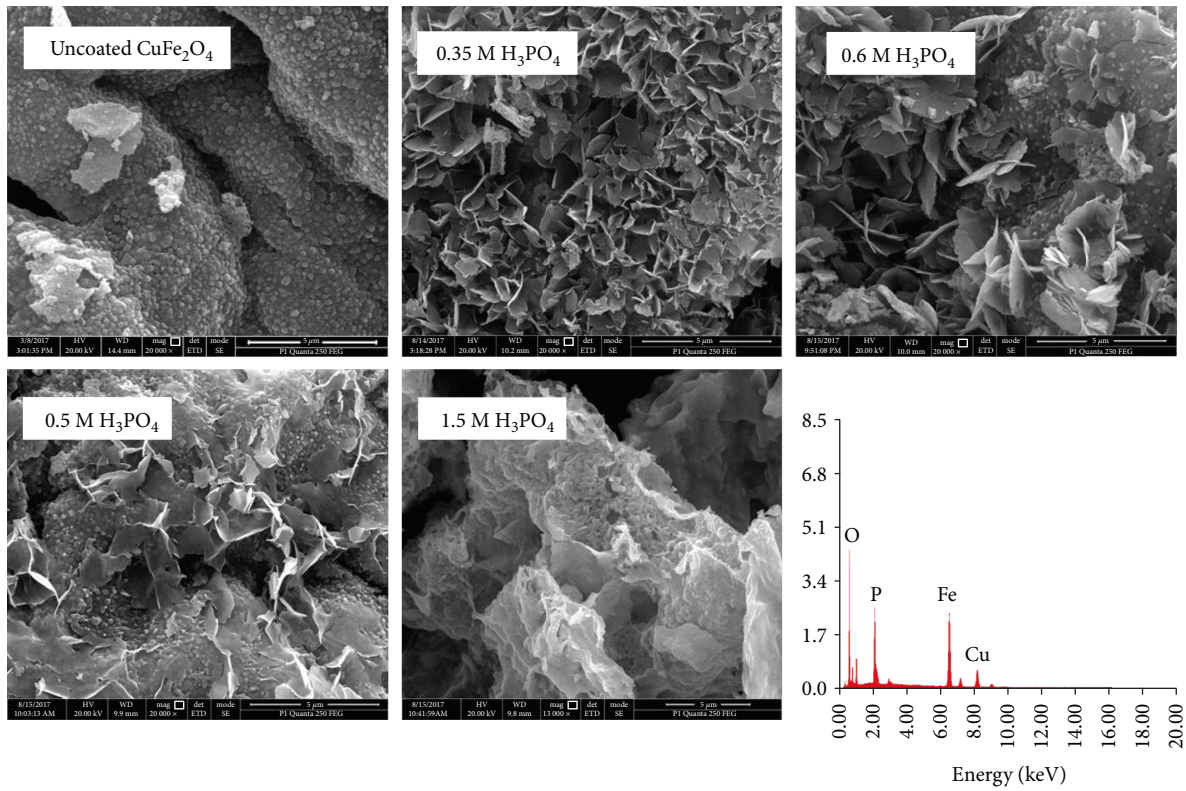

Figure 3: SEM micrographs of phosphate-coated $CuFe_2O_4$ samples by treatment with 0.35, 0.6, 0.8, and 1.5 M of H_3PO_4.

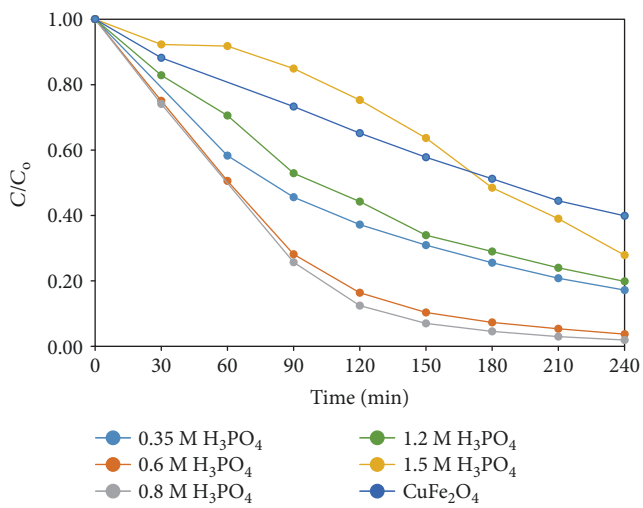

Figure 4: Catalytic activities of uncoated and phosphate-coated $CuFe_2O_4$ samples (60 mg catalyst, 25°C, no pH adjustment, no light).

nanoparticles are more active than the pure uncoated $CuFe_2O_4$ nanoparticles toward phenol degradation. This result indicates that phosphate coating enhanced the catalytic activity of the $CuFe_2O_4$ nanoparticles. The noticeable increase in the catalytic activity can be attributed to the changes in the surface morphology of the $CuFe_2O_4$ particles as observed in Figure 3. Based on Figure 4, the optimum treatments with phosphoric acid are 0.6 and 0.8 M H_3PO_4 which show the highest catalytic activities with an almost complete removal of phenol after 4 hours. Interestingly, treatments with 0.35 and 1.2 M H_3PO_4 showed lower catalytic activities than the 0.6 and 0.8 M treatments. The lowest catalytic activity among the phosphate-coated samples is observed for the sample treated with 1.5 M H_3PO_4. Based on the XRD and SEM results, the treatment with 1.5 M H_3PO_4 significantly affected the $CuFe_2O_4$ structure as compared with other H_3PO_4 treatments.

In the Fenton-type catalytic reactions [19], the degradation of phenol only occurs when the catalyst and H_2O_2 are simultaneously present in the solution. The reaction of H_2O_2 with the catalyst generates hydroxyl radicals ($HO^{\bullet}$) which attack and degrade phenol. The catalyst in the present study, phosphate-coated $CuFe_2O_4$, activates the decomposition of H_2O_2 to hydroxyl radicals. The degradation of phenol occurs as a result of a reaction between hydroxyl radicals ($HO^{\bullet}$) and phenol (PhOH). By removing a hydrogen atom from the phenol ring, new radicals ($PhO^{\bullet}$) are produced which may further decompose to intermediate products, carbon dioxide, and water:

$$\begin{aligned} H_2O_2 + \text{catalyst} &\longrightarrow 2HO^{\cdot} \\ HO^{\cdot} + PhOH &\longrightarrow PhO^{\cdot} + H_2O \\ PhO^{\cdot} + H_2O_2 &\longrightarrow \text{intermediate products} \longrightarrow CO_2 + H_2O \end{aligned} \quad (4)$$

Table 1: Reaction rate constants of phenol degradation using different phosphate-coated $CuFe_2O_4$ catalysts.

$CuFe_2O_4$ treatment	k (min^{-1})	R^2
0.35 M H_3PO_4	0.0090	0.9955
0.6 M H_3PO_4	0.0149	0.9899
0.8 M H_3PO_4	0.0208	0.9883
1.2 M H_3PO_4	0.0103	0.9969
1.5 M H_3PO_4	0.0068	0.8402

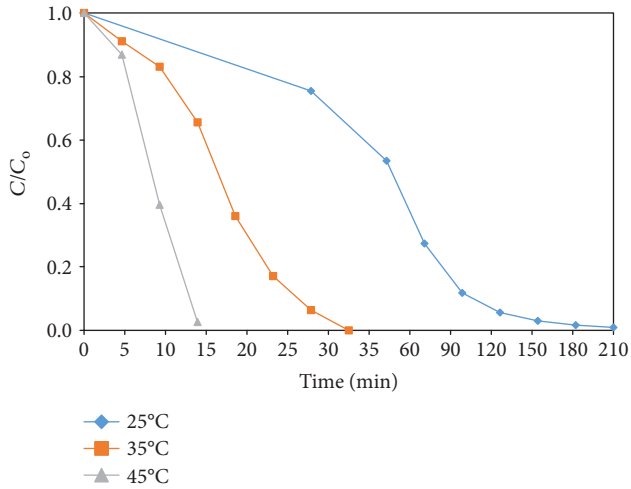

Figure 5: Effect of reaction temperature on phenol degradation using 0.8 M phosphate-coated $CuFe_2O_4$ (60 mg catalyst, no pH adjustment, no light).

Table 2: Reaction rate constants of phenol degradation at different reaction temperatures.

Reaction temperature (°C)	k (min^{-1})	R^2
25	0.0208	0.988
35	0.0888	0.900
45	0.2584	0.913

Figure 4 indicates that the catalytic performance of $CuFe_2O_4$ nanoparticles toward phenol degradation has significantly enhanced after the phosphate-coating process. Clearly, phosphate-coated $CuFe_2O_4$ nanoparticles promote a faster phenol degradation as compared to pure uncoated $CuFe_2O_4$ ones. The higher catalytic activity of the phosphate-coated $CuFe_2O_4$ nanoparticles is most likely due to a higher production of hydroxyl radicals, which in turn facilitates the degradation of phenol. Therefore, it can be suggested that the phosphate coating enhanced H_2O_2 decomposition to OH radicals. The rate of degradation reactions followed first-order kinetics (Equation 3) with respect to phenol concentration. The reaction rate constants are listed in Table 1.

3.2.1. Effect of Reaction Temperature. Figure 5 shows the effect of reaction temperature on the degradation of phenol using phosphate-coated $CuFe_2O_4$ catalysts. The reactions were investigated at three different temperatures which are 25°C, 35°C, and 45°C. The obtained results indicate that phenol degradation increased by increasing the reaction temperature. Reactions at 45°C and 35°C showed complete

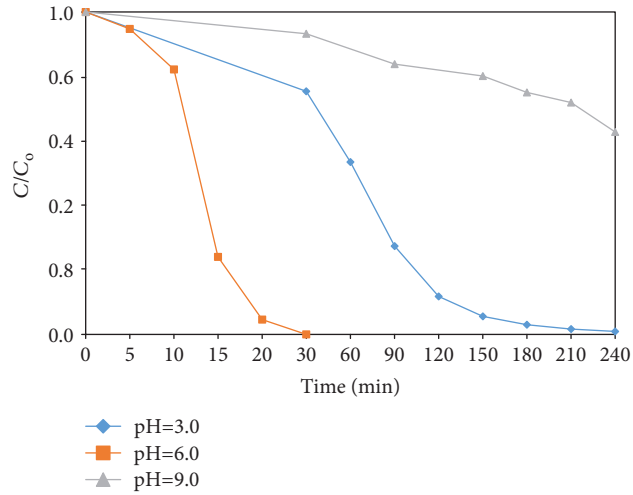

Figure 6: Effect of pH on phenol degradation using 0.8 M phosphate-coated $CuFe_2O_4$ (60 mg catalyst, 25°C, no light).

Table 3: Reaction rate constants of phenol degradation at different pH values.

pH	k (min^{-1})	R^2
3.0	0.1506	0.897
6.0	0.0208	0.988
9.0	0.0018	0.972

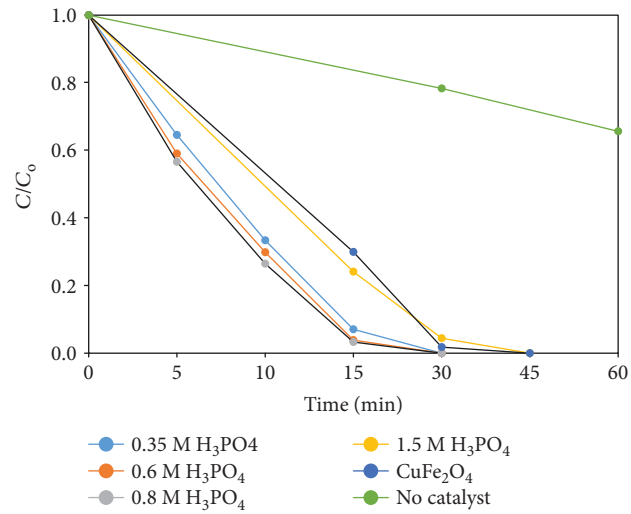

Figure 7: Photocatalytic activities of uncoated and phosphate-coated $CuFe_2O_4$ samples (60 mg catalyst, 25°C, no pH adjustment).

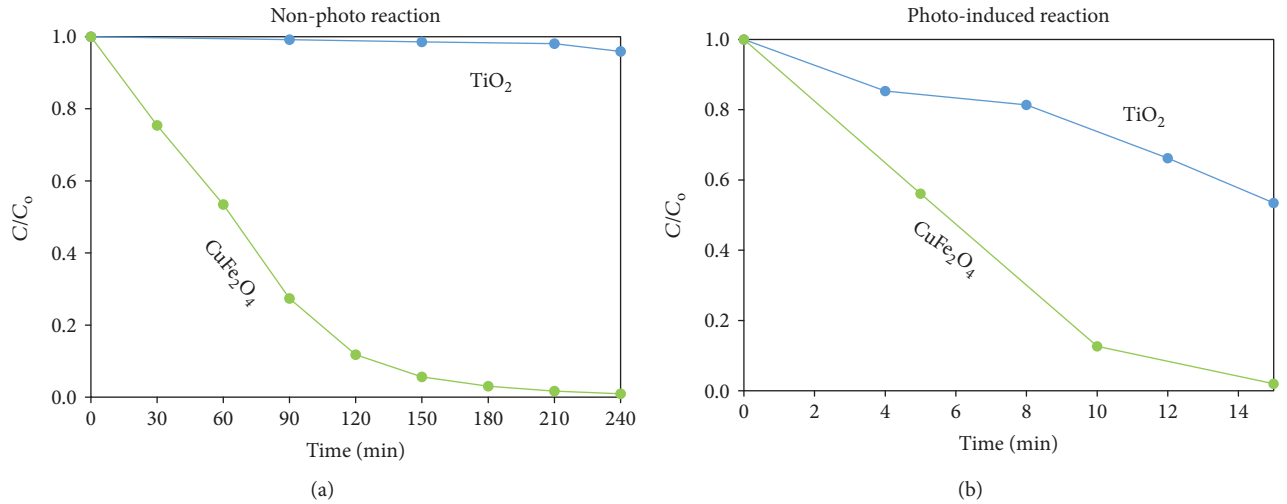

FIGURE 8: Nonphotocatalytic (a) and photoinduced catalytic (b) reactions using phosphate-coated $CuFe_2O_4$ (0.8 M H_3PO_4) and TiO_2 catalysts (60 mg catalyst, 25°C, no pH adjustment).

degradation of phenol less than 20 and 35 minutes, respectively. While at 25°C, the reaction consumed about 4 hours to achieve a complete degradation of phenol. High reaction temperatures activate the decomposition of H_2O_2 to OH radicals and, consequently, increase the degradation of phenol [37–40]. Table 2 presents the reaction rate constants calculated at the three reaction temperatures. Clearly, the reaction at 45°C exhibited the highest reaction rate constant value indicating the fastest degradation of phenol.

3.2.2. Effect of Initial pH. The role of solution pH on the degradation of phenol was investigated. The pH value of the reaction solution was adjusted using 0.1 M NaOH and 0.1 M HCl, and the results are presented in Figure 6. Clearly, the highest degradation of phenol was achieved at the acidic conditions (pH = 3), whereas the degradation at alkaline conditions (pH = 9) proceeded with a much lower extent. The high catalytic activity at acidic conditions can be due to metal leaching from the catalyst to the solution and, consequently, performing as a homogeneous catalyst. At alkaline conditions, H_2O_2 decomposition produces O_2 and H_2O, rather than OH radicals, which reduces the degradation extent of phenol [19, 41]. The rate constants for the reaction at different pH values are listed in Table 3.

Additionally, the photocatalytic activities of the $CuFe_2O_4$ catalysts were investigated, and the results are presented in Figure 7. The results reveal that the activity of the $CuFe_2O_4$ catalysts increased after the phosphate coating, which indicates that such coating also enhanced the photocatalytic performance of the $CuFe_2O_4$ nanoparticles. Moreover, comparing Figure 7 with Figure 4 clearly reveals that phenol degradation significantly increased for the photoinduced reaction. After 30 min, a complete phenol removal was achieved under photocatalytic conditions, whereas only about 25% of phenol removal was reached under nonphotocatalytic conditions. Such a difference in the phenol removal suggests that the phosphate-coated $CuFe_2O_4$ nanoparticles can be considered as efficient photocatalysts. The relevant photoinduced reactions at the catalyst surface causing the degradation of phenol can be expressed as follows:

$$\text{catalyst} + h\nu \longrightarrow e_{CB}^{-} + h_{VB}^{+} \quad (5)$$

$$H_2O_2 + e_{CB}^{-} \longrightarrow OH^{-} + HO^{\cdot} \quad (6)$$

$$\text{PhOH} + h_{VB}^{+} \longrightarrow \text{intermediate products} \longrightarrow CO_2 + H_2O \quad (7)$$

$$\text{PhOH} + e_{CB}^{-} \longrightarrow \text{intermediate products} \longrightarrow CO_2 + H_2O \quad (8)$$

$$\text{PhOH} + HO^{\cdot} \longrightarrow \text{intermediate products} \longrightarrow CO_2 + H_2O \quad (9)$$

In equation 5, the photocatalytic reaction is initiated when the catalyst absorbs a photon which leads to the promotion of an electron in the conductive band (e_{CB}^{-}) and formation of a positive hole in the valence band (h_{VB}^{+}) [42]. The e_{CB}^{-} and h_{VB}^{+} exhibit powerful reducing and oxidizing properties, respectively. In addition to $HO^{\bullet}$, e_{CB}^{-} and h_{VB}^{+} facilitate the degrading of phenol as presented in equations 6, 7, 8, and 9.

TiO_2 is considered one of the most used catalysts in many industrial processes. Therefore, the catalytic activities of phosphate-coated $CuFe_2O_4$ and TiO_2 towards phenol degradation were compared. The results of photoinduced and nonphotoreactions are presented in Figure 8. Under nonphotoreaction conditions (Figure 8(a)), an almost complete phenol degradation was achieved after 4 hours using the phosphate-coated $CuFe_2O_4$ catalyst, while only 5% of phenol was removed by TiO_2. This result clearly indicates that the coated $CuFe_2O_4$ catalyst is more active than the TiO_2 catalyst. Compared to Figure 8(a), Figure 8(b) highlights the higher degradation of phenol by both catalysts, TiO_2 and $CuFe_2O_4$, under photoinduced reaction conditions. However, the phosphate-coated $CuFe_2O_4$ catalyst is still significantly more active than TiO_2 towards phenol.

4. Conclusions

The prepared sol-gel autocombustion $CuFe_2O_4$ nanoparticles were coated with phosphate after treatment with H_3PO_4 of different concentrations. The phosphate-coated $CuFe_2O_4$ catalysts' purity, crystallinity, composition, and morphology were analyzed using SEM, EDS, FTIR, and XRD techniques. Their catalytic and photocatalytic activities were investigated for the degradation of phenol using HPLC. The obtained results showed that phosphate-coated $CuFe_2O_4$ catalysts are excellent heterogeneous Fenton-type catalysts for phenol degradation and exhibited higher catalytic activities compared with pure uncoated $CuFe_2O_4$ catalysts. The higher catalytic performance after phosphate coating can be due to improving the morphological, electronic, and chemical properties of pure uncoated $CuFe_2O_4$ catalysts. The phosphate-coated catalysts performed better in the acidic medium (pH = 3) and at high temperatures (e.g., T = 35 and 45°C) with complete removal of phenol. Moreover, the phosphate-coated $CuFe_2O_4$ catalyst showed higher activity compared to the TiO_2 catalyst which is one of the most used catalysts in industrial processes.

Data Availability

The XRD, SEM, and IR data used to support the findings of this study are included within the article.

Conflicts of Interest

The authors declare that they have no conflicts of interest.

Acknowledgments

The authors are grateful to the Research Office at Khalifa University of Science and Technology, SAN campus, Abu Dhabi, UAE, for funding project # LTR14013.

References

[1] M. Luan, G. Jing, Y. Piao, D. Liu, and L. Jin, "Treatment of refractory organic pollutants in industrial wastewater by wet air oxidation," *Arabian Journal of Chemistry*, vol. 10, pp. S769–S776, 2017.

[2] S. Mancipe, F. Tzompantzi, H. Rojas, and R. Gómez, "Photocatalytic degradation of phenol using MgAlSn hydrotalcite-like compounds," *Applied Clay Science*, vol. 129, pp. 71–78, 2016.

[3] B. H. Diya'uddeen, W. M. A. W. Daud, and A. R. Abdul Aziz, "Treatment technologies for petroleum refinery effluents: a review," *Process Safety and Environmental Protection*, vol. 89, no. 2, pp. 95–105, 2011.

[4] Z. Zhu, F. Liu, H. Zhang, J. Zhang, and L. Han, "Photocatalytic degradation of 4-chlorophenol over Ag/MFe2O4 (M ¼ Co, Zn, Cu, and Ni) prepared by a modified chemical co-precipitation method: a comparative study," *RSC Advances*, vol. 5, no. 68, pp. 55499–55512, 2015.

[5] Y. Pang and H. Lei, "Degradation of p-nitrophenol through microwave-assisted heterogeneous activation of peroxymonosulfate by manganese ferrite," *Chemical Engineering Journal*, vol. 287, pp. 585–592, 2016.

[6] I. Ibrahim, I. O. Ali, T. M. Salama, A. A. Bahgat, and M. M. Mohamed, "Synthesis of magnetically recyclable spinel ferrite (MFe2O4, M=Zn, Co, Mn) nanocrystals engineered by sol gel-hydrothermal technology: high catalytic performances for nitroarenes reduction," *Applied Catalysis B: Environmental*, vol. 181, pp. 389–402, 2016.

[7] L. P. Lingamdinne, J. R. Koduru, Y.-L. Choi, Y.-Y. Chang, and J.-K. Yang, "Studies on removal of Pb (II) and Cr (III) using graphene oxide based inverse spinel nickel ferrite nano-composite as sorbent," *Hydrometallurgy*, vol. 165, pp. 64–72, 2016.

[8] W. Zhou, W. Guo, H. Zhou, and X. Chen, "Phenol degradation by Sulfobacillus acidophilus TPY via the meta -pathway," *Microbiological Research*, vol. 190, pp. 37–45, 2016.

[9] A. Haddadi and M. Shavandi, "Biodegradation of phenol in hypersaline conditions by Halomonas sp. strain PH2-2 isolated from saline soil," *International Biodeterioration & Biodegradation*, vol. 85, pp. 29–34, 2013.

[10] S. Munirasu, M. A. Haija, and F. Banat, "Use of membrane technology for oil field and refinery produced water treatment—a review," *Process Safety and Environmental Protection*, vol. 100, pp. 183–202, 2016.

[11] C. Oh, S. Ji, Y. Cheong, and G. Yim, "Applicability of electrochemical wastewater treatment system powered by temperature difference energy," *Journal of Hazardous Materials*, vol. 351, pp. 108–116, 2018.

[12] P. Ma, H. Ma, S. Sabatino, A. Galia, and O. Scialdone, "Electrochemical treatment of real wastewater. Part 1: effluents with low conductivity," *Chemical Engineering Journal*, vol. 336, pp. 133–140, 2018.

[13] M. Kurian and D. S. Nair, "Heterogeneous Fenton behavior of nano nickel zinc ferrite catalysts in the degradation of 4-chlorophenol from water under neutral conditions," *Journal of Water Process Engineering*, vol. 8, pp. e37–e49, 2015.

[14] X. Yang, J. Li, T. Wen, X. Ren, Y. Huang, and X. Wang, "Adsorption of naphthalene and its derivatives on magnetic graphene composites and the mechanism investigation," *Colloids and Surfaces A: Physicochemical and Engineering Aspects*, vol. 422, pp. 118–125, 2013.

[15] S. J. Kulkarni, R. W. Tapre, S. V. Patil, and M. B. Sawarkar, "Adsorption of phenol from wastewater in fluidized bed using coconut shell activated carbon," *Procedia Engineering*, vol. 51, pp. 300–307, 2013.

[16] A. L. N. Mota, L. F. Albuquerque, L. T. C. Beltrame, O. Chiavone-Filho, A. Machulek Jr., and C. A. O. Nascimento, "Advanced oxidation processes and their application in the petroleum industry: a review," *Brazilian Journal of Petroleum and Gas*, vol. 2, no. 3, pp. 122–142, 2008.

[17] L. F. Liotta, M. Gruttadauria, G. Di Carlo, G. Perrini, and V. Librando, "Heterogeneous catalytic degradation of phenolic substrates: catalysts activity," *Journal of Hazardous Materials*, vol. 162, no. 2-3, pp. 588–606, 2009.

[18] Q. Cheng, V. Pavlinek, A. Lengalova, C. Li, T. Belza, and P. Saha, "Electrorheological properties of new mesoporous material with conducting polypyrrole in mesoporous silica," *Microporous and Mesoporous Materials*, vol. 94, no. 1-3, pp. 193–199, 2006.

[19] N. Hamdan, M. Abu Haija, F. Banat, and A. Eskhan, "Heterogeneous catalytic degradation of phenol by a Fenton-type reaction using copper ferrites (CuFe2O4)," *Desalination and Water Treatment*, vol. 69, pp. 268–283, 2017.

[20] B. Sahoo, S. K. Sahu, S. Nayak, D. Dhara, and P. Pramanik, "Fabrication of magnetic mesoporous manganese ferrite nanocomposites as efficient catalyst for degradation of dye pollutants," *Catalysis Science & Technology*, vol. 2, no. 7, p. 1367, 2012.

[21] Y. Wu, M. Yang, S. Hu, L. Wang, and H. Yao, "Characteristics and mechanisms of 4A zeolite supported nanoparticulate zero-valent iron as Fenton-like catalyst to degrade methylene blue," *Toxicological and Environmental Chemistry*, vol. 96, no. 2, pp. 227–242, 2014.

[22] Y. Wu, H. Yao, S. Khan, S. Hu, and L. Wang, "Characteristics and mechanisms of kaolinite-supported zero-valent iron/-H2O2System for nitrobenzene degradation," *CLEAN - Soil, Air, Water*, vol. 45, no. 3, 2017.

[23] S. Hu, H. Yao, K. Wang, C. Lu, and Y. Wu, "Intensify removal of nitrobenzene from aqueous solution using nano-zero valent iron/granular activated carbon composite as Fenton-like catalyst," *Water, Air, & Soil Pollution*, vol. 226, no. 5, 2015.

[24] R. Sharma, S. Bansal, and S. Singhal, "Tailoring the photo-Fenton activity of spinel ferrites (MFe2O4) by incorporating different cations (M = Cu, Zn, Ni and Co) in the structure," *RSC Advances*, vol. 5, no. 8, pp. 6006–6018, 2015.

[25] M. M. Rashad, R. M. Mohamed, M. A. Ibrahim, L. F. M. Ismail, and E. A. Abdel-Aal, "Magnetic and catalytic properties of cubic copper ferrite nanopowders synthesized from secondary resources," *Advanced Powder Technology*, vol. 23, no. 3, pp. 315–323, 2012.

[26] M. A. Haija, A. I. Ayesh, S. Ahmed, and M. S. Katsiotis, "Selective hydrogen gas sensor using CuFe 2 O 4 nanoparticle based thin film," *Applied Surface Science*, vol. 369, pp. 443–447, 2016.

[27] Z. Shahnavaz, P. M. Woi, and Y. Alias, "A hydrothermally prepared reduced graphene oxide-supported copper ferrite hybrid for glucose sensing," *Ceramics International*, vol. 41, no. 10, pp. 12710–12716, 2015.

[28] M. Huang, C. Wu, Y. Jiang, and M. Yan, "Evolution of phosphate coatings during high-temperature annealing and its influence on the Fe and FeSiAl soft magnetic composites," *Journal of Alloys and Compounds*, vol. 644, pp. 124–130, 2015.

[29] D.-D. Qin, Q.-H. Wang, J. Chen et al., "Phosphorus-doped TiO2nanotube arrays for visible-light-driven photoelectrochemical water oxidation," *Sustainable Energy & Fuels*, vol. 1, no. 2, pp. 248–253, 2017.

[30] N. O. Gopal, H.-H. Lo, T.-F. Ke et al., "Visible light active phosphorus-doped TiO2 nanoparticles: an EPR evidence for the enhanced charge separation," *The Journal of Physical Chemistry C*, vol. 116, no. 30, pp. 16191–16197, 2012.

[31] H. Feng, M.-H. Zhang, and L. E. Yu, "Phosphorus-doped TiO2 catalysts with stable anatase-brookite biphase structure: synthesis and photocatalytic performance," *Journal of Nanoscience and Nanotechnology*, vol. 13, no. 7, pp. 4981–4989, 2013.

[32] C. Regmi, Y. K. Kshetri, D. Dhakal, J. K. Sohng, F. Rosei, and S. W. Lee, "Insight into phosphate doped BiVO4 heterostructure for multifunctional photocatalytic performances: a combined experimental and DFT study," *Applied Surface Science*, vol. 466, pp. 787–800, 2019.

[33] L. Kumar, P. Kumar, A. Narayan, and M. Kar, "Rietveld analysis of XRD patterns of different sizes of nanocrystalline cobalt ferrite," *International Nano Letters*, vol. 3, no. 1, 2013.

[34] Z. Li, J. Lyu, and M. Ge, "Synthesis of magnetic Cu/CuFe2O4 nanocomposite as a highly efficient Fenton-like catalyst for methylene blue degradation," *Journal of Materials Science*, vol. 53, no. 21, pp. 15081–15095, 2018.

[35] N. M. Deraz, "Production and characterization of pure and doped copper ferrite nanoparticles," *Journal of Analytical and Applied Pyrolysis*, vol. 82, no. 2, pp. 212–222, 2008.

[36] E. Ajami and K.-F. Aguey-Zinsou, "Calcium phosphate growth at electropolished titanium surfaces," *Journal of Functional Biomaterials*, vol. 3, no. 2, pp. 327–348, 2012.

[37] Z. Cheng, B. Yang, Q. Chen, Z. Shen, and T. Yuan, "Quantitative relationships between molecular parameters and reaction rate of organic chemicals in Fenton process in temperature range of 15.8 ˚C–60 ˚C," *Chemical Engineering Journal*, vol. 350, pp. 534–540, 2018.

[38] D. Zhao, X. Liao, X. Yan, S. G. Huling, T. Chai, and H. Tao, "Effect and mechanism of persulfate activated by different methods for PAHs removal in soil," *Journal of Hazardous Materials*, vol. 254-255, pp. 228–235, 2013.

[39] Y. Ji, C. Dong, D. Kong, J. Lu, and Q. Zhou, "Heat-activated persulfate oxidation of atrazine: implications for remediation of groundwater contaminated by herbicides," *Chemical Engineering Journal*, vol. 263, pp. 45–54, 2015.

[40] R. J. Shannon, M. A. Blitz, A. Goddard, and D. E. Heard, "Accelerated chemistry in the reaction between the hydroxyl radical and methanol at interstellar temperatures facilitated by tunnelling," *Nature Chemistry*, vol. 5, no. 9, pp. 745–749, 2013.

[41] P. Wang, X. Bian, and Y. Li, "Catalytic oxidation of phenol in wastewater — a new application of the amorphous Fe78Si9B13 alloy," *Chinese Science Bulletin*, vol. 57, no. 1, pp. 33–40, 2012.

[42] P. Xiong, Y. Fu, L. Wang, and X. Wang, "Multi-walled carbon nanotubes supported nickel ferrite: a magnetically recyclable photocatalyst with high photocatalytic activity on degradation of phenols," *Chemical Engineering Journal*, vol. 195-196, pp. 149–157, 2012.